The Hydrophobic Effect

Why Do Raindrops Slide off Leaves?

Dhaval A. Doshi, Erik B. Watkins, Jacob N. Israelachvili, and Jaroslaw Majewski

Many interesting phenomena occur at the surface where two materials meet, and for biological and chemical processes, one of these two materials is often water. Using neutron reflectometry to look at the interface between water and a hydrophobic surface, scientists at the Los Alamos Neutron Science Center have confirmed that water literally hovers above the hydrophobic (or water-hating) surface on a very thin, low-density water layer. The thickness of that layer is about a million times smaller than a millimeter, and it changes with the type and concentration of gas present in the liquid. The presence of a water-depleted layer at hydrophobic surfaces may have implications for many processes—from protein folding and formation of lipid membranes, relevant to biology, to new technologies for water purification and fuel cells.

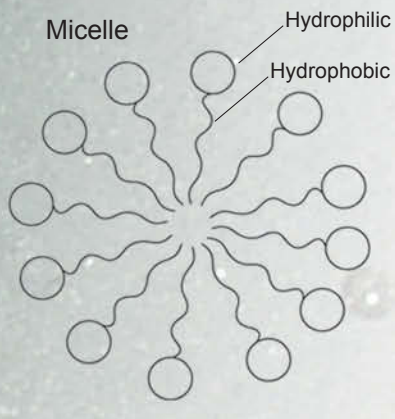

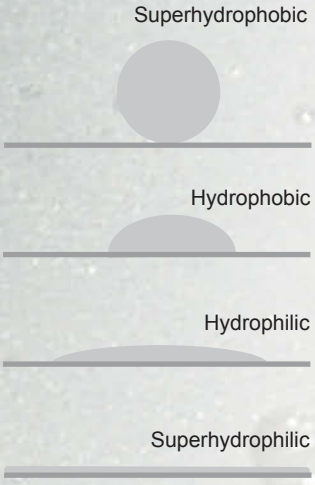

In nature, surfaces range from hydrophilic (water-loving) to hydrophobic (water-hating) or, more exactly, from superhydrophilic to superhydrophobic. The contact angle between a water droplet and the surface goes from much less than 90° for hydrophilic surfaces to much more than 90° for superhydrophobic surfaces. The latter are typically very rough. Examples include butterfly wings and the leaves of many plants. Amphiphilic molecules have hydrophilic, or polar, heads and hydrophobic, or hydrocarbon, tails. In water, they tend to assemble into closed micelles with the hydrophilic heads on the surface and the hydrophobic tails in the interior. Detergents fall into this category, enclosing dirt particles as they form micelles in water.

The interplay between water and a hydrophobic surface is found everywhere in nature. Water molecules, which tend to stick together because of the large electrical dipole forces between them, segregate from nonpolar molecules such as oil and other hydrocarbons.[1] Raindrops roll off a silane-treated windshield, and the lotus leaf is self-cleaning because of this property.

Life exists in and depends on the vicinity of water. As a result, most biological processes, to one extent or another, are shaped by the interaction between biological molecules and water. Proteins, the tiny biological machines inside our bodies, are built out of parts that are hydrophobic and hydrophilic (having an affinity for water). The way the proteins are shaped and function depends on the intricate interplay of these different parts and the water environment that surrounds them.

In engineering contexts, the hydrophobic interaction influences a wide range of phenomena, including the behavior of small particles in solution, the self-assembly of molecules into bigger complexes, the way detergents clean our clothes, oil recovery processes, the manufacture of nonstick surfaces, mineral extraction and separation, anticorrosive layers, and water flow through small pores in hydrophobic membranes. Understanding the way water flows through such pores holds the key to designing materials and processes for future water purification systems, for fuel cell membranes, and for microfluidic devices. Thus, understanding the interface between water and the hydrophobic layer (hereafter referred to as "the water-hydrophobic interface") bears not only on biological questions, such as the origin of life, but also on our future water and energy resources, which affect our national security.

But what exactly happens at a water-hydrophobic interface? Are there structural changes at the molecular level that produce the hydrophobic effect? That question has been debated for over 50 years. Yet despite the ubiquitous presence of the hydrophobic effect, its range and origin have not been resolved. A new wrinkle was added to the debate when Jacob Israelachvili and Richard Pashley (1984) discovered a long-range attractive force between two hydrophobic surfaces submerged in water. That attractive force, called the hydrophobic interaction, extends tens of nanometers (one nanometer is one billionth of a meter). Early theoretical models suggested that, at the hydrophobic-water interface, the structure of water changes to a less-dense, more-ordered phase akin to ice. More recently, images from experiments done with an atomic force microscope suggested that submicroscopic water-vapor bubbles, 50 to 500 nanometers in diameter and 5 to 50 nanometers in height, are present on some hydrophobic surfaces (Attard 2003). But the atomic force microscope is an invasive tool, introducing an additional interface into the system and additional doubts in the results.

In our recent experiments, we used a noninvasive neutron-reflectivity technique to study the water-hydrophobic interface and found a tiny cushion of low-density water between the hydrophobic surface and the bulk liquid. The water-depleted cushion appears to be only about 1 nanometer thick and decreases in thickness a few tenths of a nanometer when the water is degassed. We postulate that the layer is made of density fluctuations rather than a fixed density distribution. Instead of a constant slab of water vapors next to the surface,

[1] Dipole forces are created by the separation of negative and positive charges. Nonpolar molecules are those in which there are no separate concentrations of charges.

Figure 1. Neutron Reflectometry Experiments at LANSCE

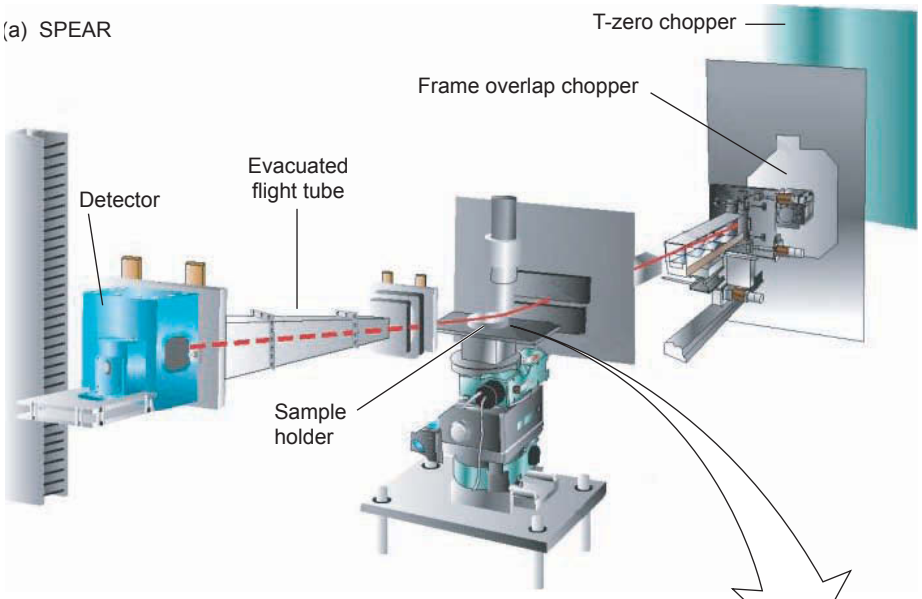

(a) The diagram shows a neutron beam being reflected from our sample at SPEAR, the Surface Profile Analysis Reflectometer at LANSCE. SPEAR is ideally suited for studies of thin (0.5 to 300 nm) organic and inorganic layers in different environments. The instrument uses an unpolarized neutron beam. Two choppers define a typical neutron wavelength range of 0.15 to 1.6 nm. Because the beam is inclined to the horizon at a very small angle (0.9°), the instrument can measure reflectivity from liquid–air interfaces. With SPEAR, good statistics can be obtained even for very low reflectivity in only 3 to 4 h.

(b) This blowup of the sample cell's interior shows the quartz-silane layer on top, a ceramic base on the bottom, and a gasket between them. It is through an inlet in the ceramic base that D_2O is injected into the enclosed space created by the gasket. The red swath indicates the path of the incident and reflected neutrons. The beam is about 1 × 10 mm and reflects from the quartz-silane and silane-D_2O interfaces.

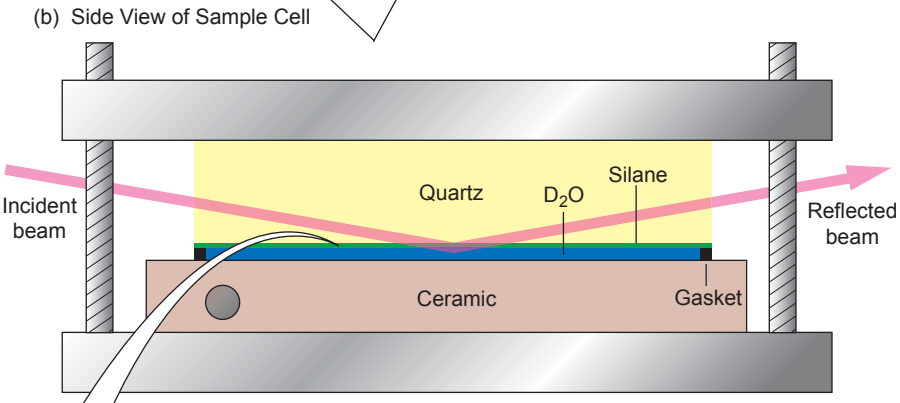

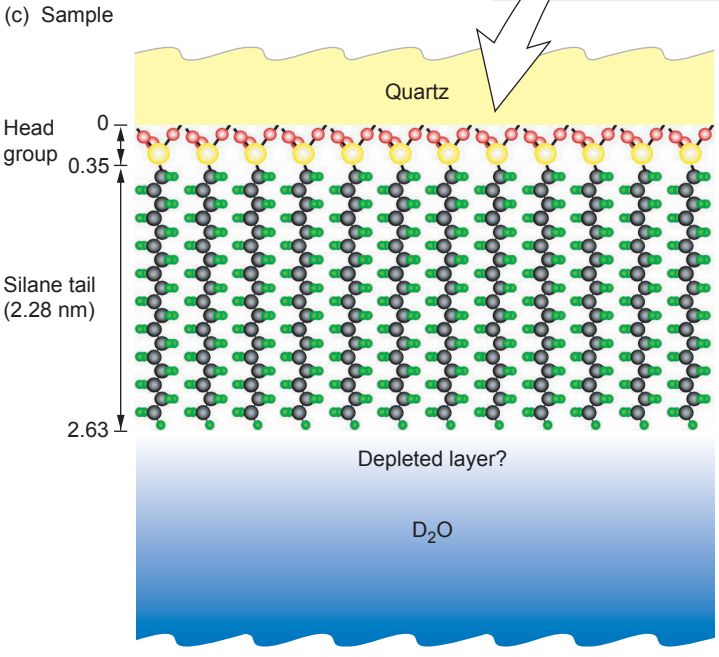

(c) This sample blowup shows the monolayer of silane molecules, each one containing a head group and an 18-carbon-chain octadecyl-tricholorosilane (OTS) tail. These molecules were deposited according to a prescribed procedure on a quartz substrate (Maoz and Sagiv 1984). Initial x-ray reflectivity measurements in air indicate that the silane portion of the monolayer has a thickness of t_{hc} = 2.28±0.05 nm, which is very close to the theoretical length for fully stretched octadecyl chains. Also shown is the adjacent layer of deuterated water with a low-density region at the hydrophobic interface.

we picture a dynamic interface at which water repeatedly touches and leaves the hydrophobic surface. Our results are consistent with recent measurements of the drag produced by flow past hydrophobic surfaces and promise to enable further quantitative understanding of hydrophobic phenomena.

Measuring the Hydrophobic-Water Interface with Neutron Reflectometry

Before our measurements, experimental evidence had generated much controversy concerning the nature and behavior of water when it meets a hydrophobic surface. Neutron reflectivity experiments at other laboratories suggested the existence of a "water-depleted," "dewetting," or "precursor gas" layer with a thickness of 1 to 4 nanometers and a mean density of 85 to 90 percent that of water. However, the systems studied were made of thick or multicomponent layers that complicated the interpretation of the results (Schwendel et al. 2003, Steitz et al. 2003). At the same time, x-ray studies were also inconclusive (Jensen et al. 2003). Disagreements regarding the accuracy of neutron and x-ray reflectivity measurements have been outlined by Phillip Ball (2003).

To understand the properties of the water-hydrophobic interface, we conducted neutron reflectivity experiments on a simple sample, containing a very thin hydrophobic layer and a water layer with high scattering contrast between the two. Figure 1 shows a schematic of our experiment at the SPEAR neutron reflectometer at the Los Alamos Neutron Science Center (LANSCE). The figure also shows details of the cell that houses the sample and the sample itself. From top to bottom, our sample consists of a highly polished quartz crystal, an atomically flat (2.28-nanometer-thick) self-assembled monolayer of silane molecules chemically attached to the quartz, and a layer of deuterated water (D_2O)—that is, water (H_2O) in which each hydrogen atom is replaced by its heavier isotope, deuterium—to create high contrast relative to the hydrophobic silane layer. The contrast we are interested in is between the neutron scattering-length densities (SLDs) of the system's components. The SLD depends on the density of the material, as well as on how well the material's atoms scatter neutrons. Both the quartz layer and the D_2O layer scatter neutrons strongly, whereas the silane layer scatters neutrons weakly. Therefore, the silane layer becomes easily discernible by neutron reflectivity.

During the experiment, incident neutrons with varying wavelengths bombard the sample at glancing angles. When they reach an interface where the density changes, more exactly, where the neutron SLD changes, some are refracted as they enter the next medium, and the remainder are reflected from the surface. The interference pattern resulting from reflections from two or more surfaces reveals the distances between those surfaces, as explained in the box "Measuring Reflectivity" on page 170. In our experiment, we were able to detect not just abrupt changes in density, but also gradual changes at the hydrophobic silane-water interface. Given the high resolution of SPEAR, changes to the density profile as small as one hundredth of a nanometer could be resolved. We repeated the reflectivity experiment using the same hydrophobic layer but with water samples containing different dissolved gases.

One might wonder why we use neutrons rather than x-rays to image a buried hydrophobic-water interface. The primary reasons are that neutrons can traverse centimeter distances in a material before and after being reflected and can sense differences in density between a hydrophobic layer and a deuterated water layer.

Experimental Results

As an example, Figure 2a shows three reflectivity curves corresponding to our hydrophobic system in contact with water under three different conditions: naturally aerated, degassed, and argon bubbled water, respectively. Because the system is extremely simple—a low neutron-scattering region (hydrocarbon molecules and water-depleted layer) is sandwiched between two high-scattering regions (quartz and deuterated water)—trends can be deduced directly from the data. In particular, the average thickness d of the low neutron-scattering region can be deduced from the values of the momentum transfer Q_z at which the reflected neutron intensity reaches a minimum (Kjaer 1994). The thickness is given by $d = 2\pi/Q_{z,\min}$ (refer to the box "Measuring Reflectivity"). Figure 2a shows minima at three different Q_z values corresponding to the different types of dissolved gas in the deuterated water. In all three cases, the thickness of the low-reflectivity region is larger than the maximum thickness of the hydrocarbon molecules. We interpret that increase as the presence of a low-density D_2O region adjacent to that layer. Such a low-density D_2O region would have a reflectivity well below that of deuterated water and thus would appear to increase the thickness of the hydrocarbon layer.

To obtain a more detailed density profile for the low neutron-scattering region, we developed a model of the density profile and determined the free parameters by fitting the data. Figure 2b shows the layers of constant thickness and scattering-length density used to describe the hydrocarbon chains and the region of

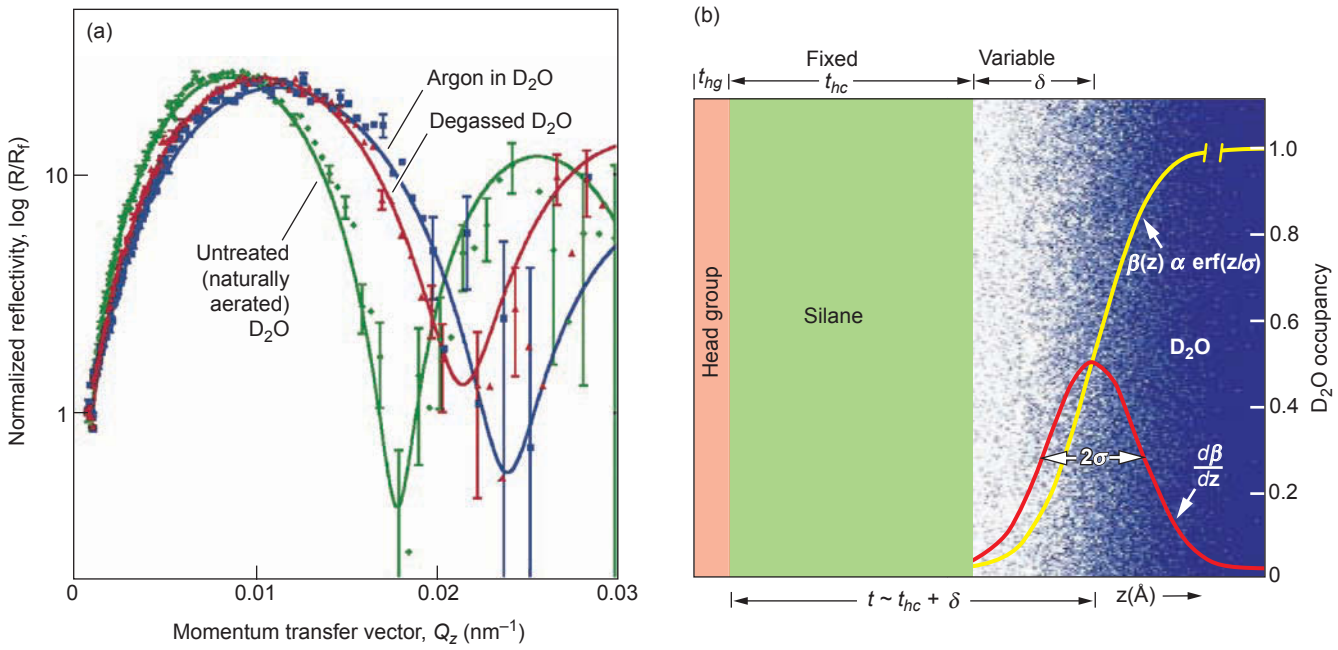

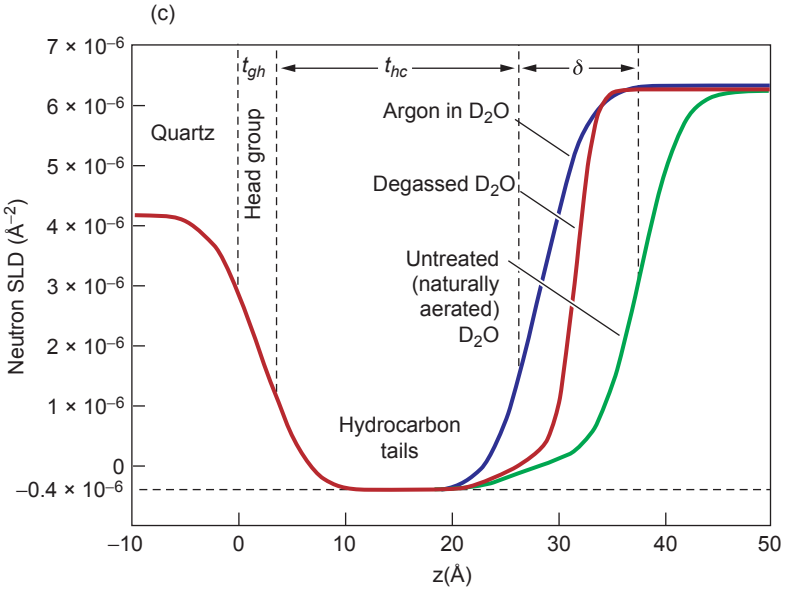

Figure 2. Reflectivity Results and SLD Profiles for Three Cases

(a) Shown here are normalized reflectivity curves for the silane layer in contact with three different D_2O layers: naturally aerated (green), degassed (red), and argon-bubbled (blue) D_2O. The thickness of the reflecting layer can be deduced directly from the value of Q_z at which the reflected intensity has a minimum value, or $t = 2\pi/Q_{z,min}$. In all three cases, the thickness of the low-density region is greater than that of the silane layer. Also, the low reflectivity layer decreases in thickness from naturally aerated, to degassed, and then to argon-bubbled D_2O. The solid curves represent fits to the reflectivity data using our variable slab-model of the SLD profile of the sample described in (b). Note that we plot Fresnel-normalized reflectivity R/R_F vs Q_z to compensate for the sharp decrease in the reflectivity with increased momentum transfer Q_z, as described by Fresnel's law: $R_F \alpha Q_z^{-4}$. Representative error bars are based on the error propagation of the Poisson statistics. (b) The simple model for the SLD profile of the sample specifies constant widths for the head group of the silane chains and the silane hydrocarbon tails. The model allows a variable width for the reduced-density D_2O layer and specifies a sigmoidal density profile of the form erf(z/σ) for the average in-plane scattering-length density $\beta(z)$ (yellow curve). The sigmoidal profile is the integral of the Gaussian with full width 2σ that describes the interfacial profile (orange curve). The mid-point of the sigmoidal curve is offset by δ from the hydrocarbon-water interface. The yellow curve shown here and the blue background density represent the SLD profile that best fit the reflectivity data for the naturally aerated layer shown in (a). (c) The plots of the in-plane average coherent scattering length density (SLD) profiles $\beta(z)$ correspond to the neutron reflectivity fits (solid curves) shown in (a). The lines at z = 0 and z = 2.63 nm represent the average positions of the silane monolayer. The line at 3.76 nm represents the 50% water density (midpoint of the sigmoidal profile) for naturally aerated D_2O.

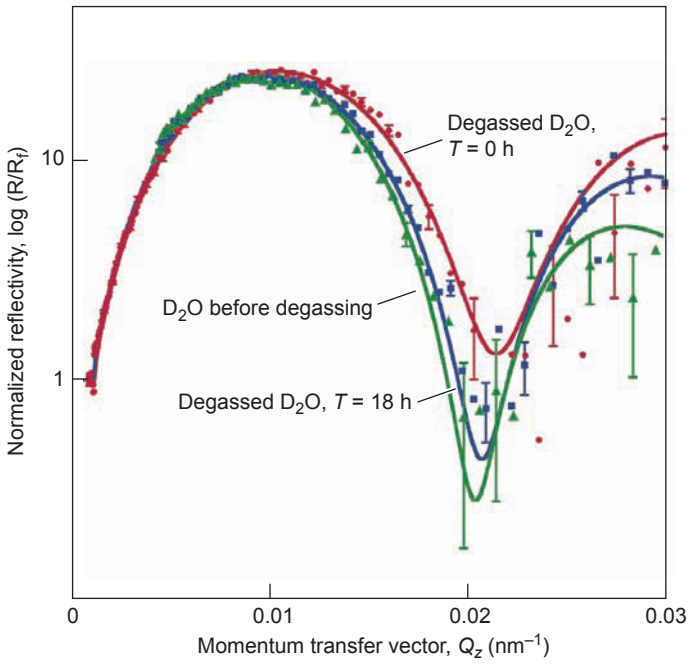

Figure 3. Reversibility of the Effects of Aeration
These neutron reflectivity curves for naturally aerated D_2O, vacuum degassed D_2O, and the degassed sample after allowing air to diffuse back into the D_2O for 18 h show that the effects of aeration on the thickness of the reduced-density layer are reversible.

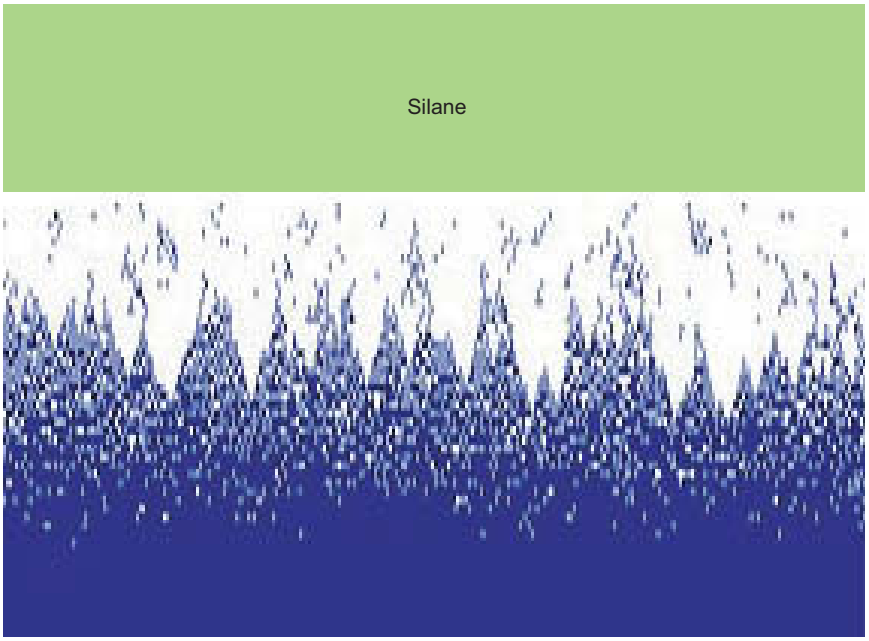

Figure 4. Density Fluctuation of the Reduced-Density Region
Our experiments suggest that the depleted-water region consists of a water surface with fluctuating density. The image shown here is dynamic, showing waves of water that tap on the hydrophobic surface.

variable thickness δ used to describe the region of reduced water density. More exactly, the reduced-water-density region was represented by an S-shaped (sigmoidal) density function with a variable width σ and variable midpoint distance δ measured from the silane surface. At δ, the water density is half the bulk value. The results of fitting this model to the data yield the solid curves in Figure 2a. The curves in Figure 2c display the scattering length density profiles obtained from fitting the neutron reflectivity data for each case in Figure 2a.

The values of δ indicate that the low-scattering region is always well above the 2.28-nanometer thickness of the hydrophobic layer. Because the hydrocarbon chains are fully extended, there appears to be a layer of reduced water density from 0.2 to 1.1 nanometers. Deuterated water bubbled with argon had the smallest reduced-density layer; the largest was for naturally aerated D_2O, whereas D_2O bubbled with carbon dioxide fell in between. To test for reversibility, we removed some of the dissolved gas from D_2O and allowed air to diffuse back in, while performing neutron reflectivity measurements. Figure 3 shows the results from this study. The shift of the position of $Q_{z,\min}$ in the normalized reflectivity back toward the original position (before degassing) 18 hours after reexposing the sample to air clearly demonstrates the effects of changing the dissolved gas concentration and the reversibility of the depleted-water-layer phenomena.

A Dynamic Interpretation

These neutron reflectivity measurements provide new clues for understanding how water behaves when it is next to a hydrophobic material. We provide an atomic-scale density profile for a simple hydrophobic surface immersed in water and observe a

Measuring Reflectivity

Neutron reflectometry is a powerful tool used to study the structure of thin, layered films. By elastically scattering a beam of neutrons off the surface of a sample, we can acquire information about the thickness, roughness, coverage, and material composition of a sample's layers perpendicular to the reflecting surface. Just like light waves, neutron waves reflect off the layer interfaces and can interfere constructively or destructively. The result is a refraction pattern analogous to the rings of color one sees when a thin layer of oil floats on top of water (refer to Figure A). By observing how the wavelength of the neutrons and their angles relative to the sample affect the reflected intensity, one can deduce the thickness and composition of the sample's layers.

We must turn to the physics of waves to understand how neutron reflectometry works. Each neutron can be described as a wave with a wavelength corresponding to its momentum. This relationship is defined by the de Broglie formula, $\lambda = h/p$, where p is the neutron's momentum, λ is the neutron's wavelength, and h is the Planck constant. Figure B shows an incident neutron reflecting from the top and bottom of a thin layer. The difference in path length between the two reflected (scattered) waves is shown in red. According to Bragg's law, constructive interference between two scattered waves will occur when the difference in path length between the two is an integral number of wavelengths. We can calculate that path length difference to show that constructive interference between neutron waves occurs when $n\lambda = 2d \sin(\theta)$, where θ is the neutron's incident angle and d is the distance between reflecting interfaces in the sample. So, the interference of neutron waves from a particular sample depends on both the wavelength λ and the angle θ. The momentum transfer vector, **Q**, is the difference between the incident and the reflected wave vectors. For reflectivity measurements, it is always in the direction normal to the reflecting surfaces and is referred to as Q_z. It combines the λ and θ variables in the form $Q_z = 4\pi \sin(\theta)/\lambda$. The reflectivity R is defined as the ratio of the number of neutrons reflected from the sample to the number of incident neutrons. By measuring a sample's reflectivity over a range of Q_z, information about the sample can be obtained for different length scales. For simple systems, the Q_z spacing between minima in the reflectivity is related to the sample's thickness by the equation $\Delta Q_z = 2\pi/d$.

In neutron reflectometry, neutrons approach the sample at a very shallow angle (0.5° to 2.0°) and are reflected from it with the same outgoing angle. For reflectivity experiments at SPEAR, the angle θ is fixed, and the incoming neutrons have a range of wavelengths and, therefore, a range of Q_z values. Plotting the intensity of reflected neutrons versus the momentum transfer Q_z, one sees an interference pattern (refer to Figure C). It looks like a series of peaks and valleys corresponding to constructive and destructive interference of neutron waves reflected from the interfaces within the sample. This interference pattern resides on the envelope of the Fresnel curve, which is the reflectivity of a perfectly sharp interface. Because the Fresnel curve decreases sharply with increasing Q_z, reflectivity data are often displayed divided by this decreasing envelope. Using a modeling process, this information can be converted into a density profile that describes the structure of the sample.

Figure A. Reflections from an Oil Film on Water
The varying thickness of the oil film creates rings of color.

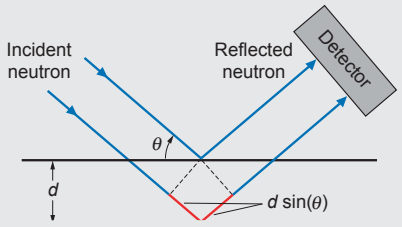

Figure B. Neutron Reflection from a Layer of Thickness *d*
The red lines show the path length difference between reflections from upper and lower surfaces.

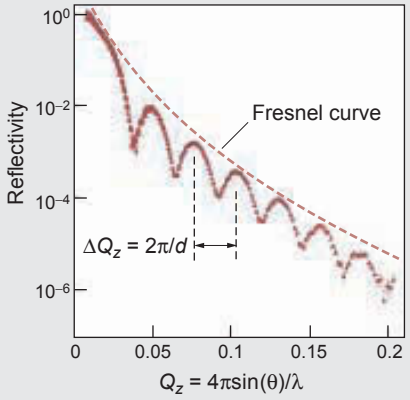

Figure C. Reflected-Neutron Intensity vs Momentum Transfer
The distance between peaks yields a layer of thickness *d*.

depleted-water region extending from 0.2 to 1.1 nanometers from the surface. Further, the extent of this depleted region was found to depend on both the concentration and type of gas dissolved in the water. Some of our more-recent studies point to additional factors that influence the extent of the depleted-water region, including pressure, temperature, and salt concentration.

A possible description of the depleted-water region is that it is made up of large, flat pockets of water vapor. However, such nanobubbles would have to cover 90 percent of the surface and have an average height less than 1.1 nanometers; under those conditions, the internal pressure of the nanobubbles would be too high for them to be thermodynamically stable. Therefore, such a picture of static bubbles does not make good physical sense. Instead, we suggest that this region consists of a water surface with a fluctuating density (refer to Figure 4). One can imagine a much more dynamic scene, where tentacles and waves of water dance upon the hydrophobic surface. ■

Acknowledgments

This work was supported by Los Alamos National Laboratory and by the U.S. Department of Energy Office of Basic Energy Science.

Further Reading

Attard, P. 2003. Nanobubbles and the Hydrophobic Attraction. *Adv. Colloid Inter. Sci.* **104** (1–3): 75.

Ball, P. 2003. How to Keep Dry in Water. *Nature* **423** (6935): 25.

Baptiste, A., A. Gibaud, J. F. Bardeau, K. Wen, R. Maoz, J. Sagiv, and B. M. Ocko. 2002. X-ray, Micro-Raman, and Infrared Spectroscopy Structural Characterization of Self-Assembled Multilayer Silane Films with Variable Numbers of Stacked Layers. *Langmuir* **18** (10): 3916.

Christenson, H. K., and P. M. Claesson. 2001. Direct Measurements of the Force between Hydrophobic Surfaces in Water. *Adv. Colloid Inter. Sci.* **91** (3): 391.

Cottin-Bizonne, C., B. Cross, A. Steinberger, and E. Charlaix. 2005. Boundary Slip on Smooth Hydrophobic Surfaces: Intrinsic Effects and Possible Artifacts. *Phys. Rev. Lett.* **94** (5): 056102.

Granick, S., Y. Zhu, and H. Lee. 2003. Slippery Questions about Complex Fluids Flowing Past Solids. *Nature Mater.* **2** (4): 221.

Israelachvili, J. N., and R. M. Pashley. 1984. Measurement of the Hydrophobic Interaction between Two Hydrophobic Surfaces in Aqueous Electrolyte Solutions. *J. Colloid Interface Sci.* **98** (2): 500.

Jensen, T. R., M. Ø. Jensen, N. Reitzel, K. Balashev, G. H. Peters, K. Kjaer, and T. Bjørnholm. 2003. Water in Contact with Extended Hydrophobic Surfaces: Direct Evidence of Weak Dewetting. *Phys. Rev. Lett.* **90** (8): 086101.

Kjaer, K. 1994. Some Simple Ideas on X-ray Reflection and Grazing-Incidence Diffraction from Thin Surfactant Films. *Physica B* **198** (1–3): 100.

Lauga, E., M. P. Brenner, and H. A. Stone. 2005. Microfluidics: The No-Slip Boundary Condition. (To appear as Chapter 15 in *The Handbook of Experimental Fluid Mechanics*. Edited by J. Foss, C. Tropea, and A. Yarin. New York: Springer-Verlag.)

Leung, K., A. Luzar, and D. Bratko. 2003. Dynamics of Capillary Drying in Water. *Phys. Rev. Lett.* **90** (6): 065502.

Maoz, R., and J. Sagiv. 1984. On the Formation and Structure of Self-Assembling Monolayers.—I. A Comparative ATR-Wettability Study of Langmuir-Blodgett and Adsorbed Films on Flat Substrates and Glass Microbeads. *J. Colloid Interface Sci.* **100** (2): 465.

Meyer, E. E., Q. Lin, and J. N. Israelachvili. 2005. Effects of Dissolved Gas on the Hydrophobic Attraction between Surfactant-Coated Surfaces. *Langmuir* **21** (1): 256.

Pratt, L. R., and D. Chandler. 1977. Theory of the Hydrophobic Effect. *J. Chem. Phys.* **67** (8): 3683.

Schwendel, D., T. Hayashi, R. Dahint, A. Pertsin, M. Grunze, R. Steitz, and F. Schreibers. 2003. Interaction of Water with Self-Assembled Monolayers: Neutron Reflectivity Measurements of the Water Density in the Interface Region. *Langmuir* **19** (6): 2284.

Steitz, R., T. Gutberlet, T. Hauss, B. Klösgen, R. Krastev, S. Schemmel et al. 2003. Nanobubbles and Their Precursor Layer at the Interface of Water against a Hydrophobic Substrate. *Langmuir* **19** (6): 2409.